The Visual Computer
https://doi.org/10.1007/s00371-025-03986-7

RESEARCH

Real-time immersive haptic sculpting with elastoplastic virtual clay

Peng Yu[1] · **Zhiyang Ji**[1] · **Aimin Hao**[1] · **Yang Gao**[1]

Accepted: 1 May 2025

Abstract
Virtual sculpting has evolved significantly, yet existing tools often neglect material physics and haptic rendering critical for realism. This paper presents a real-time immersive sculpting system that integrates material point method (MPM)-based elastoplastic material simulation with haptic rendering. To model the complex elastoplastic behaviors and the seamless interactions with tools within the MPM framework, we address this limitation by introducing a deformation-aware function that dynamically adjusts PK1 stress computation. It enables a seamless shift from elasticity to plasticity in the material. And for the realistic haptic feedback, we proposed a novel three-degree-of-freedom haptic rendering algorithm by solving a nonlinear least-squares problem. Additionally, to alleviate the visual artifacts of the marching cubes approach for surface reconstruction during cutting operations, we proposed a dual-field marching cubes algorithm that maintains topological consistency through adaptive isosurface blending. The experiments demonstrate real-time performance (78.4 FPS at 104k particles) and superior penetration resistance compared to the traditional MPM approach. A user study with 32 participants revealed significantly lower cognitive load (NASA-TLX, $p < 0.05$) and higher usability (SUS, $p < 0.05$), with haptic force correlating strongly (r=0.983) with real-world sculpting forces. The proposed framework advances immersive sculpting by unifying physical accuracy, haptic realism, and computational efficiency.

Keywords Immersive virtual sculpting · Elastoplasticity clay · Haptic rendering · Physics-based simulation

1 Introduction

Virtual sculpting serves as a critical tool in the creation of 3D assets and offers a digital platform for artistic education in virtual modeling. Typically, applications employ a mouse for model creation, utilizing brushing techniques to manipulate 3D meshes by rotating, stretching, inflating, and deflating shapes [30]. In automotive design, physical clay modeling plays a key role in vehicle surface development, enabling clear communication between modelers and designers while ensuring high-quality outcomes [31]. Physical clay exhibits elastoplastic behavior, balancing elastic resistance to deformation with permanent plastic reshaping once yield stress is surpassed. Without accurately modeling elastoplasticity, the virtual sculpture would be either too rigid (if only elasticity is considered) or too easily deformed (if only plasticity is considered), neither of which would provide a realistic experience for the artist.

Recently, some outstanding studies explored immersive sculpting within VR environments, focusing on the simulation of clay-related materials [37]. Barreiro et al. [1] developed a viscoelastic clay model by establishing viscous and elastic constraints based on the position-based dynamics (PBD) method. They also proposed an ultrasound haptic rendering algorithm that enables users to perceive tactile forces when interacting with the clay. Meyer et al. [21] utilized the finite element method (FEM) to model elastoplastic materials. Although FEM is known for its accuracy, it is computationally intensive and does not support cutting operations, which are essential for virtual clay sculpting. Li et al. [15] introduced a unified smoothed particle hydrodynamics (SPH) framework capable of modeling a range of non-Newtonian behaviors. However, reliance on an offline solver restricts its application in real-time VR environments. Mandal et al. [18] developed a physics-based virtual sculpting system with realistic haptic feedback, featuring an efficient, remeshing-free cutting algorithm called improved

✉ Yang Gao
gaoyangvr@buaa.edu.cn

[1] State Key Laboratory of Virtual Reality Technology and Systems, School of Computer Science and Engineering, Beijing, China

Published online: 24 May 2025

stable eXtended FEM. However, it does not support real-time interactive cutting.

Among these sculpting simulation models, the material point method (MPM) [12, 13, 16] offers a promising alternative. This hybrid framework, which combines Lagrangian and Eulerian approaches, is well suited to simulate a wide range of materials, including elastic solids, fluids, and particulate substances such as sand and snow [10, 14]. MPM excels in managing collisions and changes in object topology, which is essential for a realistic sculpting experience. Hu et al. [13] developed the Moving Least Square MPM (MLS-MPM) and the Compatible Particle-In-Cell (CPIC) method, which effectively simulate material cutting. These advancements make MPM a robust choice for VR clay sculpting, capable of handling the complex interactions required in such a dynamic environment. However, MPM implementations struggle to achieve smooth elastoplastic transitions. Fang [8] et al. proposed an implicit MPM for simulating viscoelastic and elastoplastic solids. However, it can hardly achieve real-time performance in moderate-scale scenes. To our knowledge, there is currently no related work that combines haptic rendering and MPM simulation. Deng et al. [7] introduced PhyVR, a real-time system enabling users to physically interact with various materials using virtual hands. Despite its innovative approach to material interaction, PhyVR lacks haptic force, which is crucial for a fully immersive user experience and precise manipulation of materials. Mandal et al. [19] proposed a method that not only incorporates haptic force, but also addresses the physical deformation of sculpting materials. However, their approach lacks real-time interactivity.

In this study, our study aims to deliver a seamless virtual sculpting experience combining visual and haptic feedback. We introduce a new elastoplastic model via CPIC, blending elastic and plastic behaviors to enhance material continuity during deformation, improving interactivity. In addition to physical simulations, we proposed a three-degree-of-freedom haptic rendering algorithm by solving a position-based nonlinear least-squares problem, enhancing the immersion and realism of the virtual environment. Besides, to address visual artifacts in surface reconstruction after cutting with the marching cubes method, we propose an enhanced version incorporating CPIC data. Finally, we evaluate the effectiveness of our framework through a user study conducted within the immersive VR environment. The experimental results indicate that the participants using our enhanced sculpting method completed the tasks more efficiently and experienced lower cognitive loads compared to those in the control group. Furthermore, most of the participants reported that haptic force during the carving process significantly eased task completion, affirming the benefits of our integrated approach.

2 Related work

This section begins with an overview of virtual sculpting applications, followed by an introduction to the physical simulation of engraving materials and haptic rendering approaches.

2.1 Virtual sculpting

Virtual sculpting is a critical component of many widely used 3D modeling applications. Within fully immersive VR settings, the dynamic between the sculptor and their work is redefined. This medium allows for manipulating and observing three-dimensional objects using tools that closely emulate real-world sculpting practices. Applications such as Meta 3D Sculpt [25] and Shapelab [26] facilitate user interaction through hand controllers, allowing for the stretching, scaling, and ultimate formation of ideal object shapes within VR space. Mcloughlin et al. [20] extended the application of virtual sculpting to therapeutic interventions for individuals with disabilities. Wong et al. [36] employed a parameterized electronic glove to control vertex movement on sculpted object surfaces. However, the resulting objects lack haptic feedback and the physical properties of real-world sculpting materials. Valentini et al. [33] and Lu et al. [17] created an augmented reality (AR) environment with a haptic force system for virtual sculpting. Callens et al. [4] designed a multilayered device that can act as a proxy in virtual environments to interact with virtual objects and provide haptic force. Biancolini et al. [3] developed a haptic-enabled virtual sculpting method for human bones using mesh morphing. However, it does not accurately replicate the physical properties of the sculpted materials. Mandal et al. [19] integrated the surface mesh of sculpted objects into a volume mesh based on FEM to provide haptic force, yet the system does not achieve real-time sculpting effects.

2.2 Physics-based simulation

Real-world sculpting materials like clay, marble, and wood display diverse physical properties. This paper concentrates on elastoplastic clay sculpting. Multiple physical modeling techniques have been developed to replicate these properties.

The FEM is frequently utilized for modeling elastic objects. Mandal et al. [19] employed the extended FEM (XFEM) to model sculpting materials with variability. Chitalu et al. [5]applied XFEM to simulate fractures in quasi-static elastic bodies. However, their methods do not account for plastic deformation and are too slow for real-time virtual sculpting. PBD are often used in real-time physical simulation applications, such as game engines like PhysX [24] and virtual surgery applications [23, 38], due to their unconditional stability, real-time performance, and versatility. Gao

et al. [11] introduced a unified FLIP-PBD-based simulation framework capable of simulating soft bodies and viscous fluids. However, these methods, while based on PBD, do not offer a physically accurate simulation model, as the material's stiffness is related to the simulation's time step and the number of iterations. Barreiro et al. [1] used position-based fluids (PBF) for interaction with virtual clay. However, PBF methods lack physical accuracy as material stiffness depends on simulation time steps and iterations.

The MPM model is a versatile simulation framework widely used for a broad range of multi-physics phenomena. Its inherent capabilities allow for topology changes and frictional interactions. For instance, Su et al. [29] proposed a second-order accurate simulation of phase-change viscoelastic fluids. Wolper et al. [35] implemented continuous fracture simulation for MPM materials. Gao et al. [9] presented an adaptive generalized interpolation material point method for modeling elastoplastic objects. Li et al. [16] introduced a data-driven MPM framework to accelerate the fluid–solid interface computation. Su et al. [28] proposed a unified phase-field-driven elastoviscoplastic model integrated with the MPM to simulate complex multi-phase interactions. Tu et al. [UnifiedMPM] proposed a material point method (MPM) with a generalized Kirchhoff stress tensor and pre-projection/post-correction rules to simulate hyperelasticity, viscoplasticity, and elastoplasticity. We adopts their MPM model for clay, enabling interaction between a haptic-controlled virtual burin and clay, supporting elastoplastic deformation under compression and cutting via the CPIC method.

2.3 Haptic rendering

Haptics is a key way humans sense the external world, perceiving force, temperature, material properties, and shape. The virtual coupling method is a common algorithm for generating haptic force feedback. For instance, Ortega et al. [22] proposed a six-degree-of-freedom "God Object" haptic rendering algorithm. The "God Object" represents the virtual instrument for visual display purposes. The motion of this God Object is constrained to the surface of the object, and the haptic force is calculated based on the positional difference between the God Object and the haptic device's proxy.

Wang et al. [34] proposed a constrained six-degree-of-freedom pose optimization function that aims to align the poses of the God Object and the haptic device's proxy as closely as possible, while ensuring that the God Object does not intersect with the object. After determining the position of the God Object, the spring force between it and the haptic device's proxy is calculated. Stewart et al. [27] utilized the linear complementarity relationship between velocity and constraint force at contact (Signorini–Fichera condition) to establish constraints and linearize the friction cone. Zhao et al. [39] employed a penalty approach to calculate the contact normal force and used constraint methods to calculate frictional forces to achieve the effect of static friction. They derived from the methods in [27] to linearize the friction cone. Ultimately, they modeled the problem of the interaction of rigid bodies with static friction forces as a linear programming issue, achieving real-time haptic rendering effects, and applied this method to virtual assembly applications. Daviet et al. [2, 6] proposed the discrete frictional contact problem. However, solving this problem requires an inversion of the Delassus operator. The Delassus operator is a large sparse symmetric matrix, and the entire computation process is highly time-consuming. Barreiro et al. [1] computed the target pressure field from PBF modeling of clay and proposed an improved clustering-based amplitude-modulation approach for ultrasound haptic rendering. While the user can sense the mid-air haptics, the forces (measured in millinewtons) are too weak compared to actual clay sculpting. The virtual sculpting application differs from the previously mentioned works. The virtual burin can deform a sculpted object's surface through compression and incise into the material. During this cutting process, the tool experiences pressure and friction from the object.

3 Backgrounds

To be self-contained, we briefly introduce the MLS-MPM [13] method in this section. The MPM addresses the governing equations, formulated from the conservation laws of mass and momentum, by combining the advantages of Lagrangian particles with those of Eulerian grids. The continuous medium is discretized into a set of material points, each encapsulating a small finite-material region. These material points are responsible for tracking various Lagrangian quantities over time, including position $\mathbf{x}_p$, velocity $\mathbf{v}_p$, and deformation gradient $\mathbf{F}_p$. We follow the math notion of [13] and use p, q for MPM particle indices, r, s for rigid body indices, and i, j for the grid node indices. At each time step, the mass and momentum on particles are first transferred to grid nodes (Particle to Grid, P2G). The grid velocities are then updated using the forward Euler method (Grid Update) and transferred back to the particles for subsequent advection (Grid to Particle, G2P). More details can be found in [14].

The CPIC method is an algorithm developed on top of the MLS-MPM. With CPIC, the MLS-MPM framework can simulate various new phenomena that were not supported by traditional MPM. The CPIC method uses a colored distance field (CDF) to represent the geometry and boundaries of materials. This allows for the simulation of complex phenomena such as material cutting and two-way rigid body coupling. The CDF encodes the minimum distance from each grid point to the nearest boundary, the set of nearby surfaces,

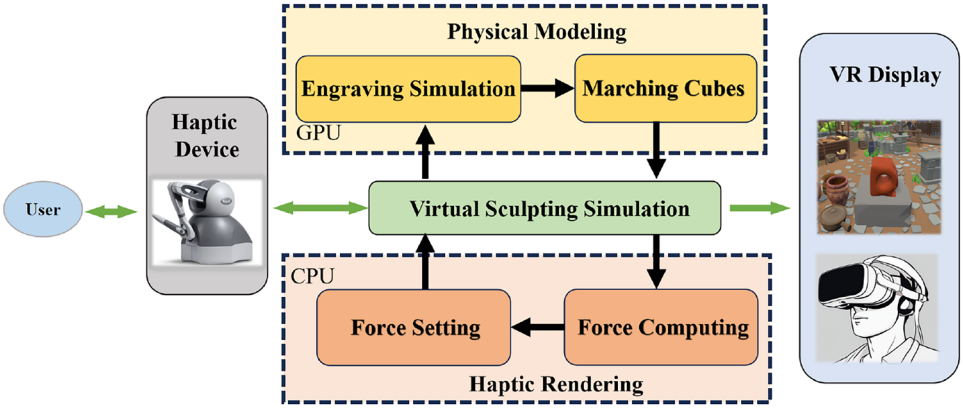

Fig. 1 The framework of our immersive virtual sculpting application. The user operates the haptic device to manipulate the virtual sculpting process. During the engraving of the clay material in virtual sculpting, the simulation may model the elastoplastic deformation of the clay. To reconstruct the clay surface, the marching cubes algorithm has been enhanced to achieve better accuracy and performance. A haptic rendering algorithm calculates the haptic force experienced by the user. The user is able to visually monitor the sculpting process through a VR headset

and the side on which the grid point is located. The compatibility condition based on CDF ensures that particles do not penetrate boundaries by applying penalty forces.

In the P2G transfer phase, compatible nodes directly contribute to mass and momentum transfer, while non-compatible nodes undergo momentum conversion through projection algorithms that translate momentum into rigid body impulses. This framework supports diverse contact boundary conditions including viscous, sliding, and separation modes. During the G2P transfer phase, velocity deficiency in non-compatible nodes is resolved through a ghost velocity extrapolation method, which reconstructs grid velocity distributions using neighboring particle velocity fields. Boundary projection corrections are applied during particle state updates, combining deformation gradient updates with penalty impulses to ensure global momentum conservation. The virtual burin is modeled as a rigid triangular surface, simplifying the CPIC method's computational complexity and implementation.

Existing studies on MLS-MPM-based elastoplastic simulations primarily target highly complex scenarios through implicit, non-real-time implementations, rendering them unsuitable for our application requirements [28] [32]. Current research lacks systematic studies on efficient real-time interaction between deformable objects and tools using the CPIC algorithm, particularly in achieving seamless, responsive elastoplastic simulations during dynamic interactions while maintaining computational efficiency.

4 Method

The pipeline of our virtual sculpting system is illustrated in Fig. 1. The user can operate the haptic device handle to control the movement of the virtual burin. When the virtual burin collides with clay, the clay can deform and be cut apart on GPU according to Sec. 4.1. At the same time, the force exerted on the virtual burin is computed and set on CPU according to Sec. 4.2. The surface of virtual clay is reconstructed using our improved marching cubes, which is depicted in Sec. 4.3.

4.1 Engraving simulation

4.1.1 Rigid–clay interaction

The traditional CPIC method primarily focuses on the simultaneous interactions between multiple rigid bodies, which are represented as discretized rigid particles. To compute the set of grid nodes, denoted as S, that are influenced by the rigid body, CPIC traverses each rigid particle and includes the surrounding $3 \times 3 \times 3$ grid nodes in S. Subsequently, for each grid node $\mathbf{x}_i \in S$, CPIC identifies the nearest rigid particle $\mathbf{x}_p$ and computes the minimum unsigned distance between $\mathbf{x}_p$ and $\mathbf{x}_i$, denoted as d_i. The complexity of calculating the minimum unsigned distance for all nodes in S is $O(n)$, where n is the number of rigid particles.

However, in virtual sculpting scenarios, the shape of the rigid body is fixed and regular. In this context, we use an oriented rigid surface as the virtual burin, enabling us to directly calculate d_i using geometric algebra. The complexity of calculating d_i is $O(1)$, significantly lower than the $O(n)$ complexity of the traditional method. Additionally, in our approach, d_i represents the minimum signed distance between the rigid particle $\mathbf{x}_p$ and the grid node $\mathbf{x}_i$. A positive value d_i indicates that $\mathbf{x}_i$ lies on the front side of the triangle, while a negative value signifies that it is on the back side of the triangle.

To determine the relative position between grid node $\mathbf{x}_i$ and the virtual burin r, we compute a tag function $T_i = sign(d_i)$ which is determined by the signed distance of the closest rigid particle d_i of grid node $\mathbf{x}_i$. The tag function T_i can take three values: 0, 1, and −1, corresponding to not near the plane, in front of the plane, and on the back of the plane. The tag information and the unsigned distance of the particles are reconstructed as T_p and d_p following [13]. We have adopted the definitions of compatible and incompatible nodes from CPIC. (For example, compatible nodes are characterized as being proximate to rigid bodies on the same side.) Compatibility will determine how particle information is updated in subsequent P2G and G2P processes, just like CPIC method. The compatibility $\delta_{i,p}$ between the particle p and the grid node i is indicated as:

$$\delta_{i,p} = \begin{cases} 1, & T_p = 0 \vee T_i = 0 \vee T_p = T_i \\ 0, & \text{otherwise} \end{cases}, \tag{1}$$

which is important for the P2G stage after cutting happens.

4.1.2 Elastoplastic model

While MLS-MPM and CPIC frameworks excel at simulating individual material behaviors (e.g., elasticity, viscosity, and plasticity), they exhibit a fundamental limitation in modeling combined elastoplastic materials in real time. To bridge this critical gap, we propose a deformation-aware elastoplastic model that dynamically modulates the first Piola–Kirchhoff (PK1) stress. This advancement establishes a new unified framework capable of simulating elastoplastic phenomena such as clay behavior, expanding the scope of physically based simulation in computer graphics. In the following sections, we systematically derive our elastoplastic model, beginning with the foundational calculation of the mass m_i^n of particle $\mathbf{x}_i$ at time t^n.

In the P2G step, near rigid surfaces r, mass (Eq. 2) and momentum (Eq. 3) from particles are only transferred to their compatible grid nodes:

$$m_i^n = \sum_p \delta_{i,p} w_{i,p} m_p, \tag{2}$$

$$(m\mathbf{v})_i^n = \sum_p \delta_{i,p} w_{i,p} \left\{ m_p \mathbf{v}_p + \left[m_p \mathrm{C}_\mathrm{p}^\mathrm{n} - \mathrm{E}_\mathrm{p}^\mathrm{n} \right] \left(\mathbf{x}_i - \mathbf{x}_p^n \right) \right\}, \tag{3}$$

where $w_{i,p}$ is the weight which determines how strongly the particle $\mathbf{x}_p$ and node interact $\mathbf{x}_i$, m_p is the mass of particle $\mathbf{x}_p$, $\mathbf{v}_p$ is the velocity of particle $\mathbf{x}_p$, and C_p^n is the affine velocity matrix.

The force impulse $\mathrm{E}_\mathrm{p}^\mathrm{n}$ delineated in Eq. 3 proceeds as follows:

$$\mathrm{E}_\mathrm{p}^\mathrm{n} = \frac{4\Delta t}{\Delta x^2} \sum_p V_p^0 \zeta\left(d_p\right) \mathbf{P}(\mathbf{F}_p^{n+1})(\mathbf{F}_p^{n+1\mathrm{T}}), \tag{4}$$

where Δt is the time step size, Δx is the grid size, V_p^0 is the undeformed volume of particle p, $\mathbf{P}(\mathbf{F}_p^{n+1})$ is the first Piola–Kirchhoff stress tensor, and $\mathbf{F}_p^{n+1}$ is the deformation gradient of particle $\mathbf{x}_p$ at time step t^{n+1}. In the original constitutive model, the $\zeta(d_p)$ does not exist. To model the elastoplasticity of clay material, we propose a novel piecewise function $\zeta(d_p)$ that adapts the material's behavior according to the distance from the interaction plane. This innovative approach enables a more realistic simulation of elastoplasticity, with softened material behavior when within a critical proximity to the virtual burin ($0 < |d_p| \leq 3\Delta x$) and abrupt transition to rigid behavior beyond this threshold:

$$\zeta(d_p) = \begin{cases} 1, & 0 < |d_p| \leq 3\Delta x \\ e^{-\frac{|d_p| - 3\Delta x}{\tau}}, & \text{otherwise} \end{cases}. \tag{5}$$

The τ in Eq. 5 can take different values according to the requirements. τ determines the transition between elasticity and plasticity. The larger the value of τ, the longer the transition distance from elasticity to plasticity, and conversely, the shorter the transition distance. In our implementation, τ is set to 0.3.

The piecewise function $\zeta(d_p)$ directly links d_p to different materials. In regions close to the interaction plane ($0 < |d_p| \leq 3\Delta x$), full activation occurs ($\zeta = 1$), leading to a lower PK1 stress and softer material behavior that facilitates plastic deformation. In contrast, outside this region ($|d_p| > 3\Delta x$), ζ rapidly decays according to $\zeta = e^{-\frac{|d_p| - 3\Delta x}{\tau}}$, approaching zero, which results in a clear transition to higher rigidity and suppresses plastic deformation, exhibiting distinct elasticity. This smooth transition captures elastoplasticity, ensuring a seamless shift between elastic and plastic regimes. Thus, the function models elastoplastic behavior with a smooth transition between the two phases.

4.2 Haptic rendering

The God Object method [22] is extensively utilized in six-degree-of-freedom rigid body haptic rendering applications. This method ensures that the graphic tool remains outside the object surface by solving an acceleration-based quasi-static nonlinear least-squares problem subject to constraints, while also maintaining the pose of the graphic tool as consistent as possible with that of the haptic tool. However, its reliance on continuous collision detection to establish constraints renders it unsuitable for real-time simulation applications.

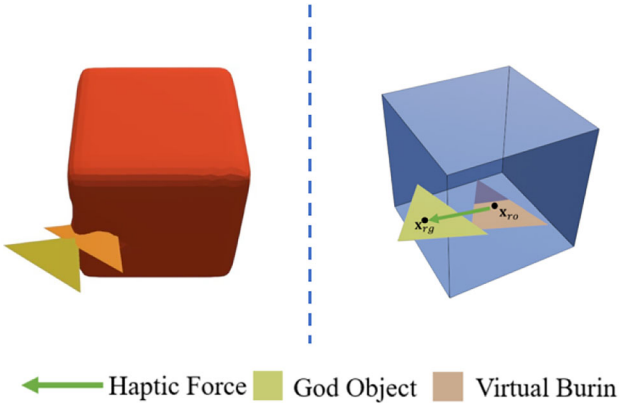

Fig. 2 The illustration depicts a haptic rendering. The God Object is constrained at the surface of virtual clay, and the orange haptic device proxy is the virtual burin. A spring force between them is computed as the haptic force

Furthermore, it exhibits stability issues in deformable object haptic rendering. In our clay cutting scenario, we introduce a novel position-based three-degree-of-freedom haptic rendering algorithm. Unlike the God Object method [22], we align the graphic tool and the haptic tool. Upon each cut, the initial configuration (God Object in Fig. 2) $\mathbf{x}_{rg} \in \mathbf{R}^3$ is recorded and serves as an anchor point to restrict the movement of the haptic tool $\mathbf{x}_{ro} \in \mathbf{R}^3$ and calculate the haptic force. The haptic rendering algorithm is divided into two stages. In the first stage, we compute the position of the virtual burin by solving a position-based nonlinear least-squares problem under non-penetration constraints, ensuring that $\mathbf{x}_{ro}$ is constrained to the surface of the clay while maintaining the positions of $\mathbf{x}_{ro}$ and $\mathbf{x}_{rg}$ as close as possible. In the second stage, the haptic force is computed based on the positions of $\mathbf{x}_{ro}$ and $\mathbf{x}_{rg}$. In the first stage, the positions of $\mathbf{x}_{ro}$ and $\mathbf{x}_{rg}$ are maintained as closely as possible, with $\mathbf{x}_{ro}$ constrained to the surface of the clay:

$$\mathbf{x}_{ro}^{t+1} = \min_{\mathbf{x}} \frac{1}{2}(\mathbf{x} - \mathbf{x}_{rg})^{\top}\mathbf{K}(\mathbf{x} - \mathbf{x}_{rg}) \quad \text{s.t.} \quad C(\mathbf{x}) \geq 0, \tag{6}$$

where $\mathbf{K}$ is a 3×3 diagonal matrix representing the translation stiffness of the haptic device, and $\mathbf{x}_{ro}^{t+1}$ is the updated position of $\mathbf{x}_{ro}$ at the next time step.

The virtual burin tool is discretized into multiple rigid particles, allowing efficient parallel computation of clay particles within a specific radius for each rigid particle on the MPM's regular background grid. To simplify collision detection and constraints for $\mathbf{x}_{ro}$, both the virtual burin particles and clay particles are modeled as spheres. The constraint function is expressed as:

$$C(\mathbf{x}_{ro}) = \|\mathbf{x}_{ro} - \mathbf{x}_q\| - (r_q + r_x) \geq 0, \tag{7}$$

where $\mathbf{x}_q$ is the center of a clay particle sphere, and r_q and r_x represent the radii of the haptic tool and clay particle spheres, respectively.

To solve the optimization function in Eq. 6, we use the Gauss–Newton method. Constraints are linearized using Taylor's theorem, followed by constructing a linear system via the method of Lagrange multipliers and solving iteratively with the Gauss–Seidel method to compute the position of $\mathbf{x}_{ro}$. Once the position $\mathbf{x}_{ro}$ is determined, the spring force between $\mathbf{x}_{ro}$ and $\mathbf{x}_{rg}$ is calculated using a traditional spring model. This force is then transmitted to the haptic device:

$$\mathbf{f} = k_h \cdot (\mathbf{x}_{rg} - \mathbf{x}_{ro}), \tag{8}$$

where k_h is the stiffness coefficient of the spring model. Unlike traditional spring models that rely solely on positional offsets, our approach dynamically adjusts the effective stiffness by incorporating the local particle density ρ derived from MPM's material point distribution. This density-aware modulation enables finer control over the graphic tool's positional constraints, particularly when encountering heterogeneous material compositions in the virtual clay. The density weighting factor $\omega(\rho)$ is integrated into the optimization function (Eq. 6) through the stiffness matrix $\mathbf{K}$, effectively correlating haptic force resolution with material microstructure. Our real-time haptic rendering algorithm significantly enhances the realism of sculpting in virtual environments and highly emulates the real-world sculpting force curve. The authenticity of the haptic force will be experimentally discussed in Sec. 5.

4.3 Improved marching cubes

The Marching Cubes (MC) algorithm is a widely used method for surface reconstruction of meshless objects. It operates by enclosing the object within a background grid, where each node stores the unsigned density of a particle. The isosurface, representing the object's surface, is defined where the unsigned density equals a specified threshold. For each cell in the background grid, the isosurface can be generated by searching a lookup table. However, a significant challenge arises in maintaining consistent topological structures when handling dynamically separated volumes, especially within the context of CPIC's material point framework.

As shown in the left panel of Fig. 3, conventional approaches that directly scatter particle information to grid nodes fail to preserve the material boundary coherence when the virtual burin partially cuts through the clay. This is because the sign ambiguity in separated regions leads to inconsistent isosurface stitching. Traditional MC assumes a single continuous scalar field, while our scenario requires handling multiple disjoint fields with shared cutting boundaries. Additionally, existing multi-volume MC variants

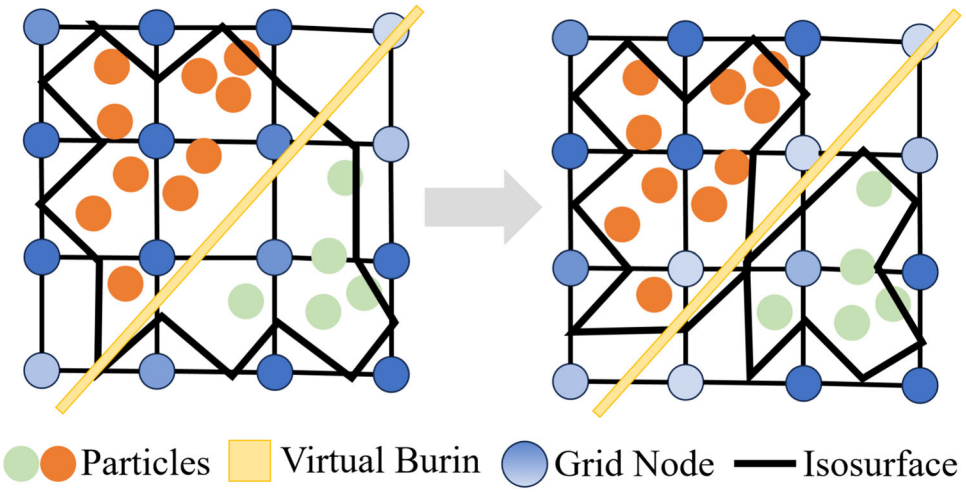

Fig. 3 The traditional MC (left) cannot reconstruct a separated isosurface like ours (right) after the virtual burin cutting through clay

cannot inherit the particle-grid coupling relationships from CPIC.

As shown in the left image of Fig. 3, if particle information is distributed to grid nodes without considering the compatibility $\delta_{i,p}$ between particle p and grid node i, the surface cannot be correctly reconstructed when the virtual cutting tool section cuts through the clay, resulting in insufficient separation. Traditional MC algorithms face difficulties in this scenario, as they rely on continuous scalar fields to define the surface. While some methods attempt to adapt the MC algorithm to handle separated objects, they fail to integrate seamlessly with CPIC. Our key innovation is the introduction of the compatibility $\delta_{i,p}$ from the CPIC computation process (Eq. 1) into the signed distance field computation. This ensures that only compatible particles and grid nodes are included in the signed distance calculation. This allows for seamless integration with the mixed Lagrangian–Eulerian framework of CPIC, while preserving the cutting interface features. In traditional MC methods, the unsigned distance of a grid node $\mathbf{x}_i$ is $c_i = \sum_p w_{i,p}$, where the weight $w_{i,p}$ is a measure of the distance from particle p to grid node $\mathbf{x}_i$. After introducing compatibility $\delta_{i,p}$, the calculation of c_i is updated to

$$c_i = \sum_p \delta_{i,p} w_{i,p}. \tag{9}$$

The improved algorithm enhances the MC algorithm's sensitivity when encountering separation planes caused by slicing, resulting in better rendering effects. As shown in Fig. 3, the incision edge is not visible using the traditional MC method when using burin cutting through a cube, whereas there is obvious grid separation when using our new method.

The MLS-MPM method is mass-conserving, but in demonstrations, substances may appear to vanish as if mass is not conserved. This paradox stems from the marching cubes rendering algorithm. The algorithm requires an artificial minimum threshold, ignoring particle clusters below this value (usually determined by grid particle density calculations). Neglecting small particle clusters avoids extending the mesh boundary for each tiny cluster, which would significantly degrade mesh quality due to their size being much smaller than the grid size. To show there is no real mass conservation violation, we provide Fig. 4, comparing the marching cubes-rendered mesh and direct particle rendering for the same frame. It can be observed that while the MC method fails to capture the underlying particle cluster, this feature remains preserved in the particle-rendered representation. To accentuate this phenomenon, we deliberately elevated the threshold parameter in the MC algorithm to preferentially disregard minor mass concentrations. This comparative analysis visually confirms the mass conservation characteristics inherent in MPM implementations.

5 Experiment and Validation

5.1 Implementation Details

We implemented our virtual sculpting system on a PC, which is equipped with an Intel i7-14700KF operating at a frequency of 3.4 GHz, 32 GB of memory, and an NVIDIA RTX 4070 Super GPU. The haptic device is Geomagic Touch as shown in Fig. 5. The HTC Vive Pro2 is utilized for the VR display. The system is built in Unity with a haptic plugin. The user can manipulate the haptic handle to control the virtual burin for sculpting the clay. We implement clay simulation using the Taichi programming language [12]. The program is then compiled into the binary Vulkan artifacts using Taichi AOT features. Then, we decompile the files into compute shaders with SPIRV-Cross which can be imported into Unity.

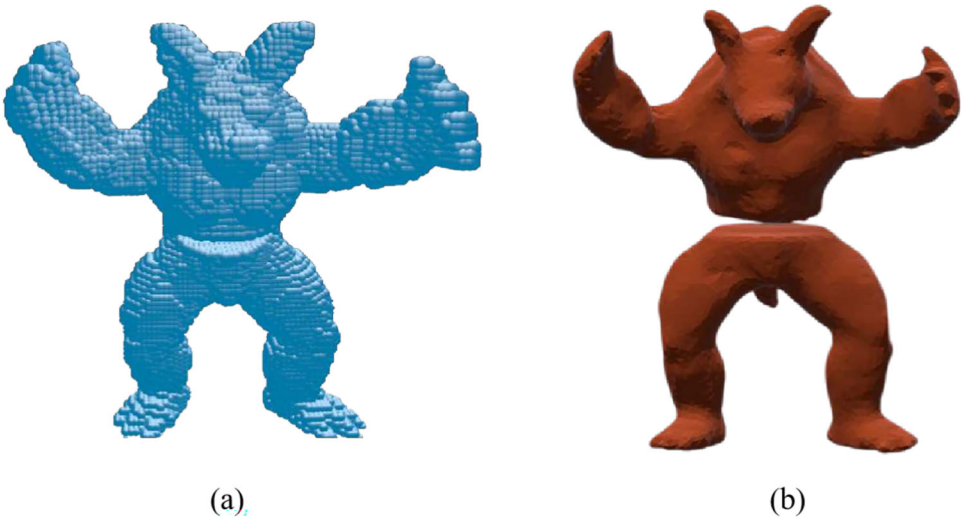

Fig. 4 Illustration of mass conservation. Figures (a) and (b) display the particles representation and reconstructed surface of an armadillo after cutting

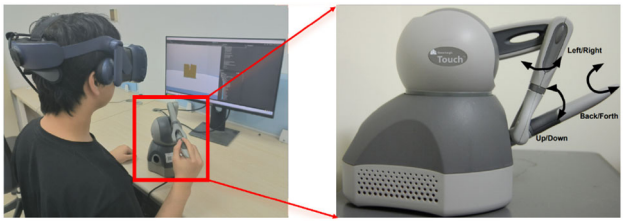

Fig. 5 Immersive virtual sculpting system setup

5.2 Evaluation

5.2.1 Ablation Studies

To validate the practical efficacy of our virtual sculpting system, we conducted a comprehensive ablation study analyzing three core innovations: CPIC optimization (CPIC-O), haptic rendering (HR), and marching cubes improvement (MCI). The study employs four experimental configurations:

- **Baseline**: Original CPIC + Standard MC + Disabled HR
- **CPIC-O**: Optimized CPIC + Standard MC + Disabled HR
- **HR**: Original CPIC + Standard MC + Enabled HR
- **MCI**: Original CPIC + Optimized MC + Disabled HR
- **Full System** Optimized CPIC + Optimized MC + Enabled HR

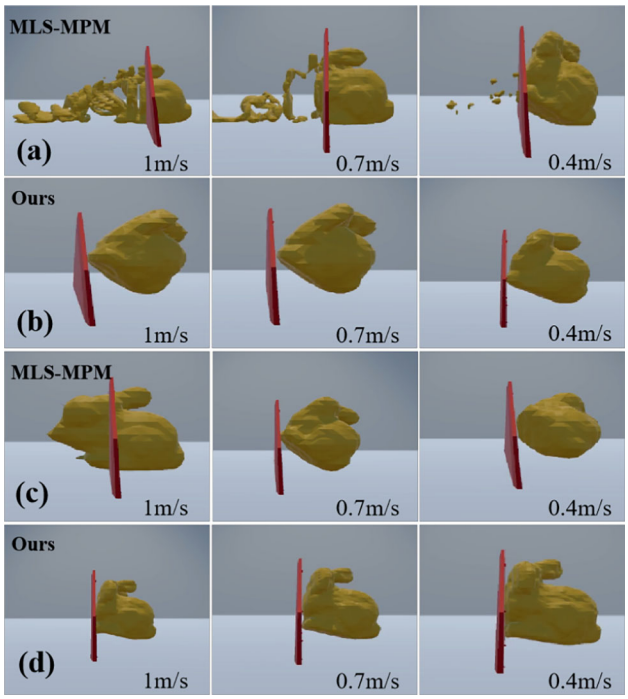

Fig. 6 Visualization of a virtual burin moving horizontally from left to right at varying speeds, interacting with bunny-shaped clay at identical frames. (a, c) Penetration patterns in conventional MLS-MPM simulations [13] with 256^3 and 128^3 grids. (b, d) Results from our method at the same grid resolutions. The sequence illustrates penetration evolution at different burin speeds, with our method ensuring non-penetrative interaction

We establish rigorous evaluation metrics through a large-scale cube cutting simulation containing 76, 820 particles in a 256^3 Eulerian grid. Statistical validity is ensured by averaging runtime measurements over 2, 700 consecutive frames, with each frame comprising 30 iterations.

Quantitative analysis reveals distinct performance characteristics: CPIC optimization introduces a marginal $1\mu s$ /iteration overhead (0.8% increase over baseline), while maintaining critical numerical stability. Notably, HR and MCI induce statistically insignificant runtime variations ($p > 0.05$, paired t test), confirming their computational neutrality. Figure 6 qualitatively validates our penetration resistance mechanism through controlled tool-clay interaction experiments. At 256^3 resolution, MLS-MPM exhibits

23±4% deeper penetration depths compared to our method after 30 frames. The introduced ζ-function enables strain-controlled plasticity, effectively limiting tool displacement even under sustained velocity inputs. Figure 7 demonstrates our geometric expressiveness through various carving tests. The haptic interface achieves sub-voxel precision (0.4× grid spacing) in feature preservation, enabling complex topology changes.

5.2.2 Haptic Rendering Evaluation

To validate the authenticity of our haptic rendering algorithm, we conducted an experiment comparing the force exerted on the clay by the sculpting tool in both the virtual and real worlds. A spring dynamometer was mounted on a six-degree-of-freedom Han's Elfin Collaborative robotic arm, which moved at a constant speed (5 mm/s) to vertically insert the dynamometer into the clay, while the computer recorded the forces. The robotic arm's speed, direction, and the clay shape in the physical world were aligned with the virtual setup to ensure a fair comparison. Both environments were configured to maintain a consistent burin position and movement. As shown in Fig. 8, the force curves from both environments were highly aligned, with the virtual world's force exhibiting a more linear trend. The Pearson correlation coefficient of 0.983 ($p < 0.01$) indicates a strong linear relationship, demonstrating that the forces in the virtual environment closely match those experienced in the real-world sculpting process, providing a realistic tactile experience.

5.2.3 Performance Analysis

We evaluated the performance across particle number and grid resolutions (64^3-200^3) through vertical cutting cubes tests as shown in Table1. All experiments were conducted with a Young's modulus of $1e5$, Poisson's ratio of 0.1, and a time step (Δt) of 2 ms with gravitational acceleration. Our empirical analysis reveals that below the 10^5-particle threshold, per-iteration computation time exhibits negligible sensitivity to particle number variations, as over 85% of the computational overhead becomes dominated by marching cubes surface reconstruction and the Unity engine's rendering pipeline.

Our systematic profiling indicates that haptic rendering latency remains stable across various operational parameters, with grid resolution and particle density exhibiting statistically insignificant impacts, as detailed in Table 1. The proposed haptic rendering algorithm achieves sub-millisecond haptic loop execution, satisfying the 2 ms stability threshold for imperceptible force discontinuities in virtual sculpting interfaces.

The apparent mismatch between cumulative subprocess timing and observed frame rates stems from Unity's main thread synchronization overhead, primarily due to rendering and physics synchronization. The low frame rate (28.1 FPS) in the third row results from the significant volumetric discrepancy between the particle system and grid-based components within our hybrid Lagrangian–Eulerian solver. This substantial mismatch induces excessive redistribution operations within the sparse matrix infrastructure, thereby compromising the computational parallelism through frequent data reallocation processes.

5.2.4 Comparisons

We compare our method with Deng et al. [7] to validate the effectiveness of our method. Deng et al. [7] introduced "interactive particles" based on MLS-MPM. The interactive particles are fully controlled by users in terms of position and velocity, while other particles participate in physical simulations as elastic object particles. Specifically, the carving tool is discretized into multiple interactive particles distributed across a triangular surface. These particles strictly follow the user's motion in terms of position while simultaneously engaging in physical simulations. The experimental comparisons between our method and Deng's method are shown in Fig. 9. The results demonstrate that our method achieves topological consistency during plastic deformation, whereas Deng's method exhibits penetration between sculpting tools and the clay.

Barreiro et al.[1] used the Ultraleap STRATOS Explore for mid-air haptic interactions in virtual clay sculpting. While functional, its ultrasonic force output was limited to 0.08 N at 50 mm, with rapid force decay, hindering realistic tactile feedback. These physical constraints fundamentally restricted the system's ability to produce realistic tactile feedback. Our methodology addresses these limitations through the adoption of the Geomagic Touch haptic interface. Experimental measurements confirm our system generates 10 times greater maximum force output (0.1 N) with significantly improved spatial consistency. The enhanced force profile enables more accurate emulation of real-world clay manipulation dynamics, particularly in simulating material resistance and tool–surface interaction forces.

5.3 User Study

In order to evaluate the usability and user experience of the virtual sculpting system, we recruited 32 participants (16 males and 16 females; mean age 22.63 (SD=3.77, range $20-32$)) for a controlled experiment. Four participants were left-handed, while the others were right-handed. Details of their VR experience can be found in Table 3. Participants were randomly divided into a control group (8 males and 8 females; mean age 22.33 ($SD = 3.72$, range $20-31$)) and an experimental group (8 males and 8 females; mean age

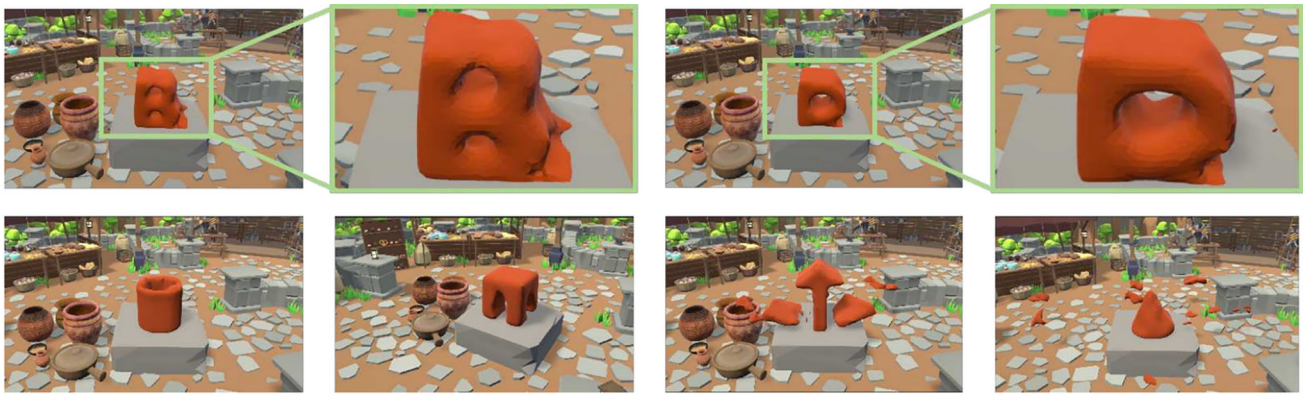

Fig. 7 A cube is engraved into various shapes, including letters "B" and "D," a cup, a square stool, an upward arrow, and a cone (from left to right, top to bottom)

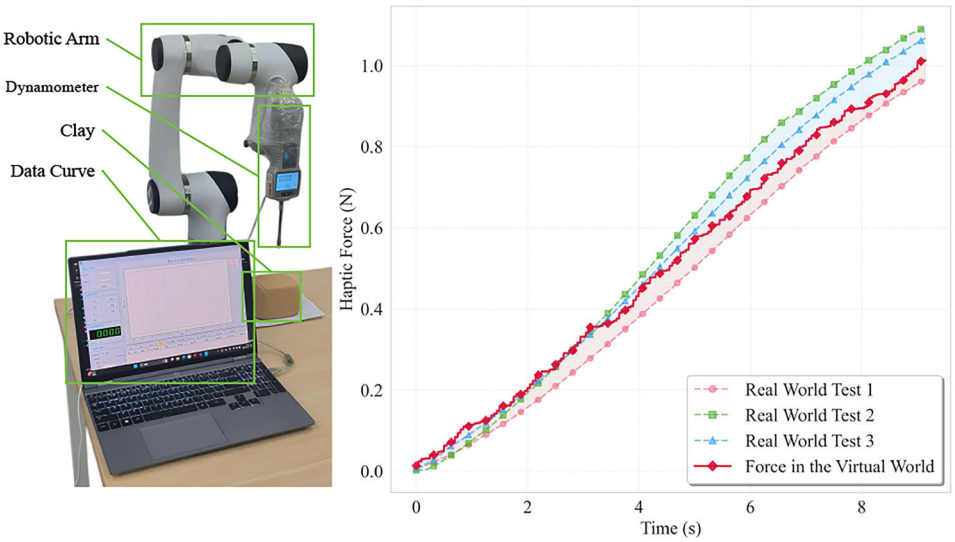

Fig. 8 Comparison of real-world sculpting force and virtual haptic sculpting force. On the left, a spring dynamometer tip controlled by a robotic arm compresses clay vertically, recording the force exerted during insertion. On the right, force curves for cube cutting with a burin are shown for both real-world (three trials) and virtual environments

Table 1 The performance comparison of different simulation scales with **Full System** configurations. The experiments were conducted with a Young's modulus of $1e5$, Poisson's ratio of 0.1, and a time step (Δt) of 2 ms

Grid resolution	Particle #	Physical simulation (ms)	Haptic rendering (s)	Marching cubes (ms)	FPS
60^3	1760	0.20	2.7e−5	3	132.8
60^3	13800	0.28	1.9e−5	4	128.9
60^3	104900	0.40	2.4e−5	9.1	28.1
120^3	1760	0.37	1.8e−5	5	128.4
120^3	13800	0.57	2.3e−5	5	127.6
120^3	104900	0.45	2.2e−5	7	96.1
200^3	1760	0.80	1.9e−5	6	113.5
200^3	13800	0.82	2.2e−5	9	110.7
200^3	104900	0.91	2.6e−5	11	78.4

Table 2 The p value and t-statistic of t test in different dimensions

Value Task Statistic	Task1 NASA-TLX	Task1 SUS	Task2 NASA-TLX	Task2 SUS
T test p value	0.0018*	0.0001*	0.0240*	0.0717
T test t-statistic	3.417	−4.406	2.375	−1.866
M test p value	0.0015*	0.0002*	0.0024*	0.0430*
M test U statistic	212.5	30.0	208.5	74.0

* p value < 0.05

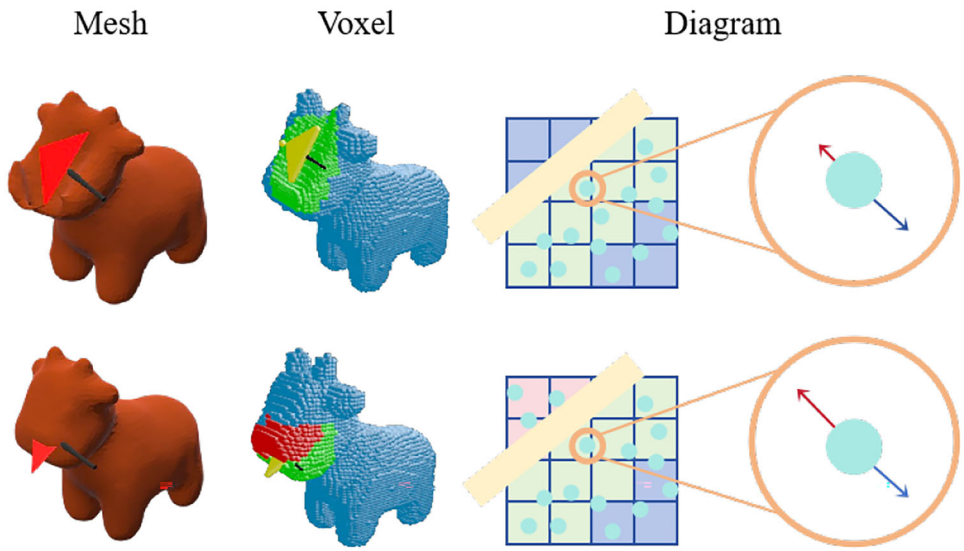

Fig. 9 Comparative simulation under consistent parameters (Young's modulus : $1e3$, Poisson's ratio : 0.1, grid density : 175^3, time step : 1 ms) with identical virtual burin motion. (Upper) Our method achieves high-plasticity clay simulation with material integrity preserved. (Lower) Deng et al.'s approach [7] exhibits noticeable material penetration artifacts. This side-by-side comparison demonstrates our method's superior capability in maintaining topological consistency during plastic deformation

Table 3 Participants' familiarity with the virtual reality environment and haptics

Device	Never	Once	Occasionally	Often
VR Experiences	15	8	8	1
Haptic Device	19	8	4	1

22.88 (SD=3.91, range 20 − 32)). In the control group, participants used a traditional MLS-MPM-based clay model to complete a virtual sculpting task without haptic force. In the experimental group, participants used our proposed sculpting system with haptic force to complete the same virtual sculpting task.

5.3.1 Study Procedure

The experiment began with participants completing a background questionnaire covering gender, handedness, and device usage experience, after which they were divided into two groups. A brief introduction to the equipment was provided, followed by two simple tasks to help participants familiarize themselves with the virtual sculpting system: vertically and horizontally dividing a cuboid into three parts. The main tasks involved sculpting a cube into the shapes of the letters M and H (Task 1) and then into a cone, cup, and chair (Task 2), with the latter being considered more difficult. Participants were shown an example of a well-completed task beforehand to clarify the objectives. After completing each task, they filled out the NASA-TLX and SUS scales to assess their cognitive load and the usability of the virtual sculpting system . The total scores from these scales were then analyzed to quantify participants' subjective evaluations.

5.3.2 Statistical Analysis

As shown in Fig. 10, the upper side of the figure presents the results for Task 1, while the lower side shows the results for Task 2. Each point represents an individual participant, with the x-axis indicating the total NASA-TLX score (where lower scores reflect lower cognitive load and a better subjective experience) and the y-axis representing the total SUS score (with higher scores indicating better system usability). To help compare the score distributions between the two tasks, marginal scales are included in the figure. For both tasks, the figure demonstrates that the participants in the experimental group generally reported a lower cognitive load (better subjective experience) and gave higher system evaluations.

As shown in Table 2, the NASA-TLX questionnaire results indicate that users in the experimental group experienced a significant reduction in cognitive load. The experimental

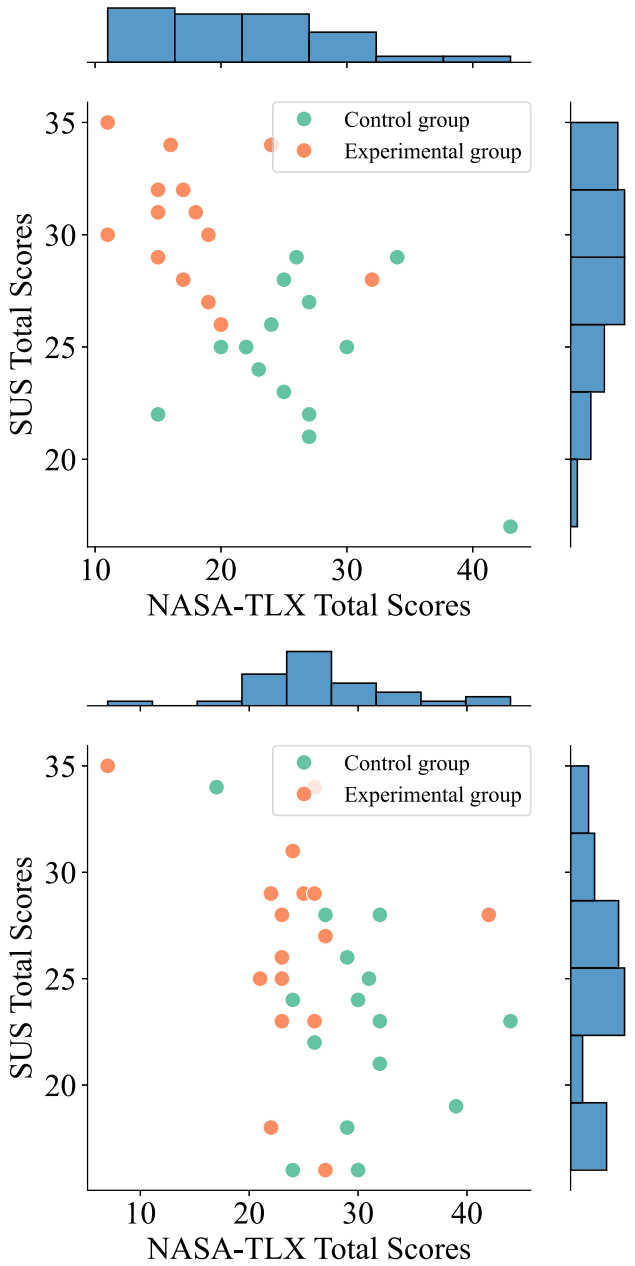

Fig. 10 Distribution of total scores on the NASA-TLX cognitive load scale (left) and the SUS usability scale (right) for both participant groups after completing Task 1 and Task 2

group reported significantly lower total NASA-TLX scores than the control group for both tasks ($p < 0.05$). This suggests that our approach effectively improves user performance, reduces the sense of failure, and lowers mental effort. Notably, the difference in self-assessed performance between the two groups was highly significant ($p < 0.001$), further emphasizing the effectiveness of our method. Besides, compared to the control group, we observed that participants in the experimental group perceived our framework to have greater usability ($p < 0.04$).

6 Conclusion

This paper proposes an immersive virtual sculpting framework with haptic rendering for simulating clay-like materials in VR environments. The deformation behavior of virtual clay is simulated through MLS-MPM, while implementing smooth elastoplastic transitions in CPIC. Haptic feedback is implemented via a three-degree-of-freedom rendering algorithm that computes haptic forces by solving a nonlinear least-squares problem. Surface reconstruction is optimized through an enhanced Marching Cubes algorithm that introduces a compatibility concept during CPIC processing, significantly improving rendering quality during cutting operations. A controlled experiment with 32 participants showed that the experimental group completed sculpting tasks faster with lower cognitive load, validating the effectiveness of our visual and haptic innovations.

Despite the advantages of our approach, there are limitations. Although the MPM approach can support a wider range of sculptable materials, we did not add richer materials (such as viscoplastic materials) due to demand and runtime efficiency limitations. In addition, current hardware runtime efficiency limits the resolution and detail fidelity. In the future, we aim to integrate our method into a standalone application running on VR headsets, enabling on-device processing.

Author Contributions Peng Yu contributed to writing—original draft, visualization, validation, and methodology and provided software. Zhiyang Ji was involved in writing—original draft, visualization, validation, and methodology and provided software. Aimin Hao contributed to project administration, resources and material, and funding acquisition. Yang Gao was involved in writing—review and editing, project administration, and funding acquisition.

Funding This work was supported in part by the National Key R&D Program of China (no. 2023YFC3604500), Beijing Natural Science Foundation under Grant (No. 4252018), National Natural Science Foundation of China (L2324214), Beijing Science and Technology Project (No. Z231100005923039), the Postdoctoral Fellowship Program of CPSF under grant number GZC-20233375, and the Guangxi Science and Technology Major Program (no. GuiKeAA24206017).

Data availability No datasets were generated or analyzed during the current study.

Declarations

Conflict of interest The authors declare no conflict of interest.

References

1. Barreiro, H., Torres, J., Otaduy, M.A.: Natural tactile interaction with virtual clay. In: 2021 IEEE World Haptics Conference (WHC), pp. 403–408 (2021)

2. Bertails-Descoubes, F., Cadoux, F., Daviet, G., Acary, V.: A nonsmooth newton solver for capturing exact coulomb friction in fiber assemblies. ACM Trans. Gr. **30**(1), 1–14 (2011)
3. Biancolini, M.E., Valentini, P.P.: Virtual human bone modelling by interactive sculpting, mesh morphing and force-feedback. In. J. Interact. Design Manuf. **12**(4), 1223–1234 (2018)
4. Callens, E., Danieau, F., Costes, A., Guillotel, P.: A tangible surface for digital sculpting in virtual environments. In: Haptics: Science, Technology, and Applications: 11th International Conference, EuroHaptics 2018, Pisa, Italy, June 13–16, 2018, Proceedings, Part II 11, pp. 157–168 (2018)
5. Chitalu, F.M., Miao, Q., Subr, K., Komura, T.: Displacement-correlated xfem for simulating brittle fracture. In: Computer Graphics Forum, vol. **39**, pp. 569–583. Wiley Online Library (2020)
6. Daviet, G.: Simple and scalable frictional contacts for thin nodal objects. ACM Trans. Gr. **39**(4), 61–1 (2020)
7. Deng, H., Li, J., Gao, Y., Liang, X., Wu, H., Hao, A.: Phyvr: physics-based multi-material and free-hand interaction in VR. In: 2023 IEEE International Symposium on Mixed and Augmented Reality (ISMAR), pp. 454–462 (2023)
8. Fang, Y., Li, M., Gao, M., Jiang, C.: Silly rubber: an implicit material point method for simulating non-equilibrated viscoelastic and elastoplastic solids. ACM Trans. Graph. **38**(4), 1–13 (2019)
9. Gao, M., Tampubolon, A.P., Jiang, C., Sifakis, E.: An adaptive generalized interpolation material point method for simulating elastoplastic materials. ACM Trans. Gr. **36**(6), 1–12 (2017)
10. Gao, Y., Li, S., Hao, A., Qin, H.: Simulating multi-scale, granular materials and their transitions with a hybrid Euler-Lagrange solver. IEEE Trans. Vis. Comput. Gr. **27**(12), 4483–4494 (2021)
11. Gao, Y., Li, S., Qin, H., Xu, Y., Hao, A.: An efficient flip and shape matching coupled method for fluid-solid and two-phase fluid simulations. Vis. Comput. **35**, 1741–1753 (2019)
12. Hu, Y.: The Taichi programming language. In: ACM SIGGRAPH 2020 Courses, pp. 1–50 (2020)
13. Hu, Y., Fang, Y., Ge, Z., Qu, Z., Zhu, Y., Pradhana, A., Jiang, C.: A moving least squares material point method with displacement discontinuity and two-way rigid body coupling. ACM Trans. Gr. **37**(4), 1–14 (2018)
14. Jiang, C., Schroeder, C., Teran, J., Stomakhin, A., Selle, A.: The material point method for simulating continuum materials. In: ACM siggraph 2016 courses, pp. 1–52 (2016)
15. Li, C., Gao, Y., He, J., Cheng, T., Li, S., Hao, A., Qin, H.: A unified particle-based solver for non-Newtonian behaviors simulation. IEEE Trans. Vis. Comput. Gr. **30**, 1998 (2023)
16. Li, J., Gao, Y., Dai, J., Li, S., Hao, A., Qin, H.: MPMNet: A data-driven MPM framework for dynamic fluid-solid interaction. IEEE Trans. Vis. Comput. Gr. **30**, 4694 (2023)
17. Lu, P., Sheng, B., Luo, S., Jia, X., Wu, W.: Image-based non-photorealistic rendering for realtime virtual sculpting. Multimed. Tools Appl. **74**, 9697–9714 (2015)
18. Mandal, A., Chaudhuri, P., Chaudhuri, S.: Interactive physics-based virtual sculpting with haptic feedback. Proc. ACM Comput. Graph. Interact. Tech. **5**(1), 1–20 (2022)
19. Mandal, A., Chaudhuri, P., Chaudhuri, S.: Interactive physics-based virtual sculpting with haptic feedback. Proc. ACM Comput. Gr. Interact. Tech. **5**(1), 1–20 (2022)
20. Mcloughlin, L., Fryazinov, O., Moseley, M., Sanchez, M., Adzhiev, V., Comninos, P., Pasko, A.: Virtual sculpting and 3d printing for young people with disabilities. IEEE Comput. Gr. Appl. **36**(1), 22–28 (2016)
21. Meyer, K.A., Skrypnyk, R., Pletz, M.: Efficient 3d finite element modeling of cyclic elasto-plastic rolling contact. Tribol. Int. **161**, 107053 (2021)
22. Ortega, M., Redon, S., Coquillart, S.: A six degree-of-freedom god-object method for haptic display of rigid bodies with surface properties. IEEE Trans. Vis. Comput. Gr. **13**(3), 458–469 (2007)
23. Pan, J., Yang, Y., Gao, Y., Qin, H., Si, Y.: Real-time simulation of electrocautery procedure using meshfree methods in laparoscopic cholecystectomy. Vis. Comput. **35**, 861–872 (2019)
24. Phsyx sdk. https://github.com/NVIDIA-Omniverse/PhysX. Accessed: 2025-02-16
25. Sculptrvr on meta quest. https://www.sculptrvr.com/. Accessed: 2025-02-16
26. Shapelab. https://shapelabvr.com/. Accessed: 2025-02-16
27. Stewart, D., Trinkle, J.C.: An implicit time-stepping scheme for rigid body dynamics with coulomb friction. In: Proceedings 2000 ICRA. Millennium Conference. IEEE International Conference on Robotics and Automation. Symposia Proceedings (Cat. No. 00CH37065), vol. **1**, pp. 162–169. IEEE (2000)
28. Su, H., Li, X., Xue, T., Jiang, C., Aanjaneya, M.: A generalized constitutive model for versatile MPM simulation and inverse learning with differentiable physics. Proc. ACM Comput. Graph. Interact. Tech. **6**(3), 1–20 (2023)
29. Su, H., Xue, T., Han, C., Jiang, C., Aanjaneya, M.: A unified second-order accurate in time MPM formulation for simulating viscoelastic liquids with phase change. ACM Trans. Gr. **40**(4), 1–18 (2021)
30. Top 3d sculpting tools for virtual reality authoring | medium by adobe. https://www.adobe.com/products/medium.html. Accessed: 2025-02-16
31. Tsuchie, S.: Interpretation of clay modeling using differential geometry and its application to surface reconstruction. Engineering with Computers pp. 1–11 (2025)
32. Tu, Z., Li, C., Zhao, Z., Liu, L., Wang, C., Wang, C., Qin, H.: A unified MPM framework supporting phase-field models and elastic-viscoplastic phase transition. ACM Trans. Graph. **43**(2), 1–19 (2024)
33. Valentini, P.P., Biancolini, M.E.: Interactive sculpting using augmented-reality, mesh morphing, and force feedback: force-feedback capabilities in an augmented reality environment. IEEE Consum. Electron. Mag. **7**(2), 83–90 (2018)
34. Wang, D., Zhao, X., Shi, Y., Zhang, Y., Hou, J., Xiao, J.: Six degree-of-freedom haptic simulation of probing dental caries within a narrow oral cavity. IEEE Trans. Hapt. **9**(2), 279–291 (2016)
35. Wolper, J., Fang, Y., Li, M., Lu, J., Gao, M., Jiang, C.: CD-MPM: continuum damage material point methods for dynamic fracture animation. ACM Trans. Gr. **38**(4), 1–15 (2019)
36. Wong, J.P., Lau, R.W., Ma, L.: Virtual 3d sculpting. J. Vis. Comput. Anim. **11**(3), 155–166 (2000)
37. Yin, Z.Y., Chang, C.S., Karstunen, M., Hicher, P.Y.: An anisotropic elastic-viscoplastic model for soft clays. Int. J. Solids Struct. **47**(5), 665–677 (2010)
38. Yu, P., Zhao, Z., Wang, R., Pan, J.: Real-time soft body dissection simulation with parallelized graph-based shape matching on GPU. Comput. Methods Progr. Biomed. **250**, 108171 (2024)
39. Zhao, D., Li, Y., Barbič, J.: 6-DoF haptic rendering of static coulomb friction using linear programming. IEEE Trans. Hapt. **11**(3), 325–337 (2018)

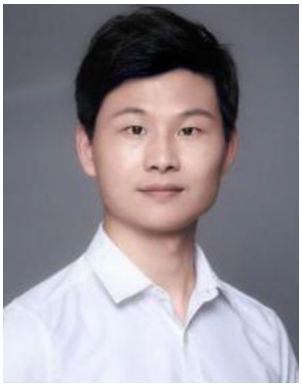

Peng Yu is currently a Postdoctoral researcher at the State Key Laboratory of Virtual Reality Technology and Systems, Beihang University. His research is centered on the innovative application of physical simulation techniques within the realm of virtual reality (VR) for surgical simulation.

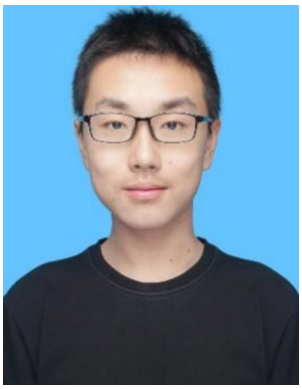

Zhiyang Ji is pursuing an undergraduate degree at the School of Computer Science and Engineering, Beihang University. His primal research interests lie in computer vision, computer graphics, and physics-based simulation.

Aimin Hao received the BS, MS, and the PhD degrees in computer science from Beihang University. He is currently a professor with Computer Science School and the associate director of the State Key Laboratory of Virtual Reality Technology and Systems, Beihang University. His research interests include virtual reality, computer simulation, computer graphics, geometric modeling, image processing, and computer vision.

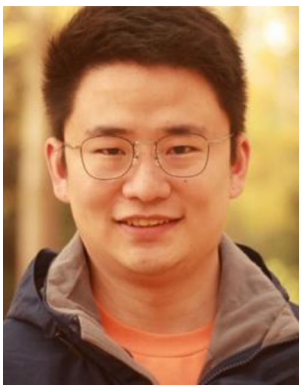

Yang Gao received the PhD degree in computer science from Beihang University in 2019. He is currently an associate professor with the State Key Laboratory of Virtual Reality Technology and Systems, Beihang University, Beijing. His research interests include computer graphics, VR or AR applications, physics-based modeling, and realistic rendering.